united nations
educational, scientific
and cultural
organization

international atomic
energy agency

the
abdus salam
international centre for theoretical physics

SMR.1313 - 3

Summer Colloquium on the Physics of Weather and Climate

Workshop on Land-Atmosphere Interactions in Climate Models

(28 May - 8 June 2001)

Modeling Land Surface Processes in Climate Models: III

"Description of Surface Heterogeneity Effects"

Filippo Giorgi
the Abdus Salam ICTP
Physics of Weather & Climate Section
Trieste
ITALY

Modeling land surface processes in climate models: III. Description of surface heterogeneity effects

Filippo Giorgi

Abdus Salam International Centre for Theoretical Physics (ICTP)
P.O. Box 586,
34100, Trieste, Italy

3.1. Introduction

One of the most important sources of uncertainty in modeling surface processes for climate models is the representation of sub-grid scale heterogeneity. In the previous lecture we have seen that state-of-the-art Earth Surface Exchange Models (ESEMs) can reproduce quite accurately the observed point-values of surface fluxes of energy and water vapor when driven by observed meteorological forcings. This is partly because of the presence of multiple parameters which can be tuned to fit specific datasets. We have also seen that for the same climatic forcing a wide range of surface response is produced by different ESEMs. Even if an ESEM was capable of perfectly reproducing the surface energy and water budget at a given location, however, coupling to an atmospheric model (AM) would still introduce a possibly large level of uncertainty because of the fine, sub-grid scale structure of the surface characteristics.

Present three-dimensional global climate models are typically run at resolutions of a few hundred km. The recent development of regional climate models, which cover only limited area domains, can allow to reach resolution of a few tens of km (e.g. Giorgi and Mearns 1991). However, the variability of surface characteristics such as vegetation type, soil properties and terrain morphology is almost fractal in nature. This is illustrated, for example, by Fig. 3.1, which presents a high resolution (1 km) map of surface vegetation types as inferred from satellite data and surface information (Loveland et al. 1991).

Usually, AMs assign at a given grid point either the dominant surface type or grid-box averaged surface characteristics. Because of the non-linear nature of many of the processes we have described in the previous two lectures, and because of the strongly varying partitioning on energy and water fluxes by different vegetation types (e.g. Seth et al. 1995), these approximations can lead to significant errors in the calculation of surface energy and water budgets. Having recognized this possible source of uncertainty, many investigators have recently attempted to address the issue of describing the effects of surface heterogeneity in ESEMs, which is the topic of this lecture.

The presentation is organized as follows. The basic problem associated with heterogeneous surface representation in ESEMs is first defined in section 3.2. Attempts to quantify the uncertainties related to surface heterogeneities and modeling approaches developed to include heterogeneous surfaces within AMs and ESEMs are reviewd in sections 3.3 and 3.4. Final considerations are then presented in section 3.5.

3.2. The problem of surface heterogeneity representation

Land surface heterogeneities occur for three basic reasons: i) variations in vegetation cover, or more generally surface type (e.g. different types of vegetation, bare soil, snow, inland water, urban areas); ii) variations in terrain morphology (e.g. slope and elevation); and iii) variations in soil characteristics (e.g. color and texture). All these three effects can strongly alter the local surface energy and water budgets, and although for some aspects they can be partially correlated, they generally vary quite independently from each other. A further degree of heterogeneity is added by the climate forcing, which can be highly variable in space and time. A typical example of this is given by summertime convective precipitation, which can strongly vary on scales of a few km or even less.

This suggests that surface heterogeneity likely spans a wide range of spatial scales. Therefore, although based on one of the criteria above it might appear that the surface is a mosaic of well defined patches, some characteristics based on the other criteria may produce within each patch a high degree of variability. An enlighting example is that of Avissar et al. (1991), who measured the plant stomatal resistance in a homogenous potato field. They found that the stomatal resistance followed a quasi log-normal distribution, mostly in response to variations of the leaf micro-environment (inclination, orientation, shading, level within the canopy, wind). For larger patches, e.g. a forest, where different species share the same environment and where terrain and soil texture can significantly vary, this effect could be far more pronounced.

These considerations allow us to define two types of heterogeneities, what we can call inter-patch and intra-patch heterogeneity. The separation between inter- and intra-patch heterogeneity cannot be strictly based on spatial scale, since we have commented that heterogeneity likely varies on a continuum of scales, but rather on the mathematical approach most suitable to treat them. Inter-patch heterogeneity can be treated with "discrete" methods, while "intra-patch" heterogeneity requires continuous approaches.

The effects that sub-grid scale surface heterogeneity has on an AM can also be roughly divided in two categories, what we here refer to as "direct" and "indirect" effects. Direct effects include the contribution of heterogenous surfaces on the grid-average fluxes of momentum, energy and water, or more generally on the grid-average energy and water budgets. Indirect effects are associated with the impact that surface fluxes from heterogenous

surfaces may have on atmospheric circulations, i.e. they are essentially dynamical in nature. Surface heterogeneities can induce mesoscale circulations, such as the sea-breeze, the vegetation-breeze, slope and urban circulations, which can affect local climate and modify the surface-atmosphere exchanges. In addition, gradients of sensible and latent heat fluxes can provide baroclinicity and moist static energy to overlying synoptic systems.

The lecture is thus organized so as to discuss separately the different approaches which have been developed to study direct and indirect effects of inter-patch and intra-patch surface heterogeneity.

3.3. Direct effects of surface heterogeneity

3.3.1 Inter-patch heterogeneity

A number of approaches of increasing complexity have been proposed to date to represent the direct effects of inter-patch heterogeneity within an AM grid cell. The simplest is that adopted by most ESEMs, e.g. SiB and BATS, and has been called the "mixture" approach (Koster and Suarez 1992). In this approach, the surface is assumed to be covered by a homogenous mixture of two surface types (e.g. tall and short vegetation, or vegetated and non-vegetated areas) with tightly coupled energy balances. The two types simultaneously interact with the soil and with an interface layer (e.g. canopy air) which in turn is interfaced with the AM bottom level. This approach has also been called "big-leaf" to reflect the assumption that a large grid area is characterized by homogeneous vegetation properties.

The resistance network for a surface variable ϕ (e.g. temperature or moisture) in the mixture approach is illustrated in Fig. 3.2a, where the subscripts a, I, g, refer to the atmospheric, interface and surface layer, respectively, r is the resistance and f_v is the fractional cover for the vegetation type i. Assuming that the interface layer has negligible capacity for the quantity ϕ, the surface-atmosphere flux $\overline{F}_\phi$ is given by

$$\overline{F}_\phi = \frac{\phi_I - \phi_a}{r_a} = \sum_i \frac{f_v^i}{r_g^i}(\phi_s^i - \phi_I) \qquad (1)$$

The mixture approach thus assumes that the different surface types are strongly coupled horizontally to yield an homogenous interface layer. This assumption is in many cases not correct. Let's assume for example that a grid point is covered by a large fraction of a wet and cool surface and a small fraction of a dry and warm surface. The boundary layer would be stable over the cool areas (i.e. over most of the grid point), resulting in small vertical fluxes. In the misture approach, this effect would dominate. On the other hand, even with a small fractional cover, because of the non-linear nature of the aerodynamic

resistance (or drag coefficient, see Fig. 1.4 of Lecture I), the instability induced by the warm and dry areas may have in magnitude an effect of the same order of magnitude of, or even greater than, that of the cool areas. Therefore, the mixture approach would lead to a relatively large error.

An alternative to the mixture approach is the "mosaic" approach, originally proposed by Avissar and Pielke (1989) and Koster and Suarez (1992), in which a grid box is divided into a number of "tiles" each having the same surface characteristics (e.g. vegetation type). Independent fluxes between surface and atmosphere are calculated for each tile (see Fig. 3.2b), so that the grid-box average flux is given by

$$\overline{F}_\phi = \sum_i \frac{f_v^i}{r_a^i + r_g^i}(\phi_s^i - \phi_a) \tag{2}$$

The mosaic approach thus assumes that different tiles do not interact with each other horizontally, but interact with the AM independently of each other.

The mosaic approach allows to account for the effects of several different surface types within an AM grid box. For each tile of the mosaic, the ESEM needs to be separately run, therefore while mosaic methods are more general than (available) mixture methods, they are also more computationally expensive. It should be noted, however, that mixture methods could be easily developed which would include multiple surface types. So the choice of mixture vs mosaic approaches is fundamentally based on the assumptions concerning the horizontal coupling between tiles.

In the original mosaic models of Avissar and Pielke (1989) and Koster and Suarez (1992) the climate forcing for each sub-grid tile was the same, and equal to the grid point averaged forcing. Thus one of the elements that determine surface heterogeneity, i.e. climate spatial variability, is lost. Pitman et al. (1992) illustrated well how this could lead to large errors. They considered a GCM cell of a few hundred km size and performed two simulations with a stand alone version of BATS. In the first, BATS was driven by grid-average forcing and in the second, precipitation was allowed to occur only over a fraction f_c of the grid point with an intensity equal to $\overline{P}/f_c$ where $\overline{P}$ is the grid box average precipitation. The latter configuration would be more realistic especially in summer conditions, when precipitation is a highly localized process. Using BATS, Pitman et al. (1992) showed that the surface water budget changed from evaporation-dominated in the first experiment to runoff-dominated in the second, mostly because greater runoff is produced at the higher precipitation rates of the second experiment. Although this result is partially dependent on the treatment of runoff in BATS (see lecture II), it emphasizes the need to include climate redistribution, especially precipitation, in surface process models.

An extension of the mosaic approach, which also includes climate redistribution within the tiles, has been proposed by Leung and Ghan (1995). In their model, tiles are not

based on vegetation or surface type, but on elevation classes, and different climate forcings are calculated for each class. In particular, the climate forcing is based on the motion of a parcel along the sloping terrain, so that different classes have different atmospheric temperature and orographically-induced precipitation forcing. The main drawback of the model of Leung and Ghan (1995) is that each elevation class behaves in the same way, regardless of it's location with respect to mountain systems (upwind or downwind), and different vegetation types within an elevation class are not recognized.

A mosaic approach which in principle allows to overcome the difficulties of the models above is that of Seth et al. (1995), defined the "vector" approach. In the vector model of Seth et al. (1995) an AM grid-box is divided into a regularly spaced subgrid of N^2 elements. Each element of the sub-grid is assigned an individual surface type, elevation and climate forcing and interacts with the atmosphere independently of the others. This model thus allows explicit spatial redistribution of vegetation, elevation and climate forcing specific to the location of the sub-grid element. It's main drawback is that an ESEM needs to be called for each of the N^2 grid points, which can be computationally rather expensive. In the work of Seth et al. (1995) a vectorized version of BATS was developed so that use of "vector"-BATS (or *V*BATS), for say a subgrid of 64 grid points, was not much more expensive than use of the original BATS. However, this approach can be also especially suitable for parallel computing architectures.

Some results from the work of Seth et al. (1995) can serve to illustrate the direct effects of the inclusion of inter-patch heterogeneity. Three areas of 300×300 km^2 size (the equivalent grid point spacing of a typical GCM) were considered in the eastern U.S. (denoted with AM1, AM2, and AM3 in Table 3.1) and two sets of experiments were performed. In the first (CONTROL experiment), BATS was run as a single grid point using the dominant vegetation type and in the second (SUBVEG experiment) a subgrid of 36 points was defined for each region, with each subgrid point characterized by a different *V*BATS vegetation type (specified from a half degree dataset). An idealized experiment was also performed in which 51% of the area was covered by forest and 49% by grass. This experiment was designed to maximize the possible error arising from using the dominant type, since forest and grass in BATS showed the largest difference in response to the same climate forcing.

The model was forced by an observed annual climatology assembled for the region at an half/hourly time step. This climatology included storm cycles of 7 day period for the cold season and daily period for the warm season. *V*BATS experiments were carried out in which climate was not redistributed thrughout the fine mesh (i.e. each sub-grid box was forced by the same climate), and in which the precipitation was spatially redistributed according to a Gaussian distribution in the cold season and to a random distribution (over 30% of the sub-grid points) in the warm season.

Table 3.1 shows the differences in annually averaged simulated fluxes of momentum, latent heat and sensible heat, along with soil moisture and runoff between the *V*BATS distributed experiments (with uniform climate forcing throughout the subgrid) and the corresponding the dominant single type BATS experiment. For the idealized experiments also the seasonal differences are shown. It can be seen that the differences can be as high as ~15-20 W/m^2 for sensible and latent heat fluxes and up to 150 N m^{-2} for momentum, with seasonal values higher than annual values. To put some of these numbers in perspective, the radiative forcing due to doubling of carbon dioxide concentration and increase of other greenhouse gases is projected to be of the order of less than 4 W/m^2 (IPCC 1994), and it has been estimated that a forcing of about 10 W/m^2 (or 10 mm/month in water flux) is sufficient to produce significant regional climatic effects (Dickinson 1992). In addition, the sensitivity of simulated runoff to inter-patch variability is very pronounced (total annual runoff in the dominant type experiments varied in the range of 20–75 mm/months for different vegetation types), which can have profound implications for the simulated surface water cycle.

3.3.2. Intra-patch heterogeneity

As already mentioned, intra-patch heterogeneity requires a continuous rather than discrete representation. The conceptual framework of this representation is presented for example by Avissar (1992) and is referred to as statistical-dynamical approach. Basically, this approach consists of defining the spatial variability of a given variable ϕ with an analitycal probability density function (PDF) $f_{pdf}(\phi)d\phi$. It is useful to select the function such that it is normalized, i.e.

$$\int f_{pdf}(\phi)d\phi = 1 \tag{3}$$

with the additional constraint that

$$\int \phi f_{pdf}(\phi)d\phi = \overline{\phi} \tag{4}$$

where $\overline{\phi}$ is the grid point average of ϕ. In principle, then the procedure is to multiply all terms in the equations of an ESEMs by $f_{pdf}(\phi)d\phi$ and integrate over the whole distribution.

As illustrative example, Avissar (1992) applies this procedure to describe the effect of intra-patch variations in stomatal resistance, r_s, on a simplified canopy model. The energy budget equation for this canopy model can be written as

$$\int f_{pdf}(r_s)(R_N + LH + SH + D_S)dr_s = 0 \tag{5}$$

or

$$\int f_{pdf}(r_s)R_N dr_s + \int f_{pdf}(r_s)LH dr_s + \int f_{pdf}(r_s)SH dr_s + \int f_{pdf}(r_s)D_S dr_s = 0 \tag{6}$$

where the terms in Eqs. (5) and (6) have been defined in the previous lectures. After a number of manipulations and simplifications, the energy balance equation reduces to

$$aT_g^4 + bT_g + cr_s e^{F(T_g)} + d = 0 \tag{7}$$

with the only unknown T_g, the canopy foliage temperature (assumed to be equal to the surface soil temperature). The coefficients $a - d$ in Eq. (7) include all terms linked to the appropriate power of T_g. The surface fluxes are then calculated with the following procedure: i) the PDF $f_{pdf}(r_s)$ is divided in a number of intervals I; ii) for each interval i, the value of r_s^i is used to calculate T_g^i by solving Eq. (7) via Newton-Raphson iteration; iii) the individual fluxes are computed by numerically calculating the integrals of Eq. (6) over the intervals i. Figure 3.3 shows the impact of five different PDFs of stomatal resistance on the simulated surface sensible and latent heat fluxes, temperature and PBL height for a 24 hour simulation. The differences between the results obtained with the various PDFs emphasize the non-linearities involved in the surface energy balance equation.

This example already points out some of the difficulties in including intra-patch heterogeneity is ESEMs. Applying the procedure of Avissar (1992) to the full set of equations included in a state-of-the-art ESEM would be extremely costly from the computational viewpoint, because the whole system would have to be solved for each numerical interval of the continuous PDF. In addition, accounting for the contribution of heterogeneity of N variables (or parameters) would entail the numerical solution of integrals of order N and the solution of the whole system of ESEM equations over I^N intervals.

Two strategies can be adopted to circumvent these difficulties. The first consists of drastically simplifying the original set of equations of an ESEM and reduce the number of independent parameters, so that the full numerical solution over the PDF distribution can be carried out. The assumption underlying this strategy is that the effects of intra-patch heterogeneity of key parameters are more important than the detailed representation of processes for an individual, "averaged", surface type.

An alternative strategy to account for intra-patch heterogeneity is to keep the complete set of ESEM equations and include PDF integration only for a few critical variables and only over some of the non-linear terms entering the equations rather than the full coupled set. From Lecture II it is evident that two of the variables which enter most non-linear terms are the soil moisture content relative to saturation and the temperature of canopy and soil. In addition, it can be expected that, because of variations in microenvironmental conditions, climatic forcing, terrain structure and soil properties, these variables may have a relatively large range of values within the scale of an AM grid box.

Therefore, a statistical-dynamical model of surface processes could begin with the assumption that surface temperature and soil water content are distributed according to analytical PDFs. If these PDFs have the properties given by Eqs. (3) and (4), by applying

the operator

$$F_{pdf} = \int X f_{pdf}(\phi) d\phi \tag{8}$$

to the various terms of the equations of an ESEM (where X in Eq. (8) represents the term of the equation), prognostic equations can be obtained for the grid-point averaged values of soil water content relative to saturation and the surface temperatures which account for the effects of non-linearities associated with these variables.

Such a model, limited to the hydrologic processes of evaporation, infiltration and runoff, was developed by Enthekaby and Eagleson (1989) who assume that the soil moisture relative to saturation within a grid box, s, follows a two-parameter gamma PDF:

$$f_{pdf}(s) = \frac{\lambda^{\alpha}}{\Gamma(\alpha)} s^{\alpha-1} e^{-\lambda s}, \qquad \lambda, \alpha, s \geq 0 \tag{9}$$

where α is inversely proportional to the coefficient of variation of the distribution. The appropriate choice of the distribution function should allow analytical integration of the non-linear terms over the full, or sub-regions of, the space domain, and is thus partially dictated by the form of the equations. As an example, the non-linearities present in the soil water equation are in the form of power functions (see Eq. (6) of Lecture II). Power functions are also the non-linearities associated with temperature, both in the infrared emission term and in the evaporation term, since the temperature dependency of the saturation vapor pressure can be accurately approximated with polynomial expressions as a function of temperature. Thus, a suitable choice of PDF which would allow analytical and computationally efficient integration of the operator F_{pdf} would be a linear or polynomial function.

The main issues concerning this approach reside in the choice of the parameters characteristic of the PDF, and in the complexity of some of the formulations typical of ESEMs, which does not allow the analytical calculation of all terms. Therefore, unless complex terms are calculated numerically, this approach would provide only a partial, first order representation of intra-patch heterogeneity, while retaining however the full complexity of the ESEM structure.

3.4. Indirect effects of surface heterogeneities

In section 3.2 we have defined the indirect effects of surface heterogeneities as those associated with organized mesoscale circulations (OMC) induced by strong horizontal gradients in surface forcings, e.g. latent and sensible heat flux. A typical example of such circulations is the sea-breeze. The physical mechanism which generates the sea-breeze is associated with the horizontal gradient in sensible heat flux induced by daytime solar heating over the cool water surface (low flux) and the warm land surface (high flux). The

diurnal evolution of the sea-breeze circulation is schematically depicted in Fig. 3.4. During the day, greater turbulent vertical mixing produces a lifting of the pressure surfaces over land compared to ocean. This generates a positive land-to-ocean horizontal pressure gradient near the surface and a negative gradient above, which initiates a near-surface on-shore circulation with an off-shore circulation aloft. This circulation tends to remove the horizontal pressure gradient in the late afternoon until it dissipates in the early evening. At night, radiational cooling over land produces a sinking of the pressure surfaces which, by a similar mechanism, initiates a reverse off-shore circulation.

Although the sea-breeze has been known and studied for many decades, it was only relatively recently that Yan and Anthes (1984) suggested that a similar OMC might be triggered by gradients in surface vegetation, e.g. grass vs forest or irrigated vs non-irrigated surfaces. Anthes (1984) suggested that such circulations might significantly affect local climate, especially in semi-arid regions, and that in fact using specified geometries for vegetation cover management could be an effective way to modify local climate (Fig. 3.5). This hypothesis was confirmed by early modeling work (Yan and Anthes 1988), and since then a multitude of studies have appeared in the literature to analyze the effect of OMCs induced by surface heterogeneities. Because of the basic two-dimensional nature of the sea-breeze process the early studies mostly employed two-dimensional mesoscale models, along with idealized background conditions (Yan and Anthes 1988, Pielke and Avissar 1990, Pielke et al. 1991). Only recently, full three-dimensional models have been used to analyze these circulations under more realistic atmospheric forcings (Lynn 1994, Seth and Giorgi 1995). In particular, the sensitivity of OMCs to different surface vegetation geometries (individual strips, alternating bands, or checkerboard of wet and dry areas) has been extensively studied.

The purpose of this lecture is not to give a comprehensive review of work on surface-induced OMCs, but rather to present and discuss the framework of the ongoing debate concerning the effects of such circulations. The basic point of this debate is that OMCs might significantly affect the fluxes of momentum, sensible heat and water vapor at the surface-atmosphere interface as well as throughout the lower troposphere (Pielke and Avissar 1990). It is also argued that the upward motions at the breeze front might trigger precipitation under suitable atmospheric conditions (Yan and Anthes 1988). If both these effects are climatologically significant, then the need is there for parameterizing them in climate models.

The basic mathematical framework to represent fluxes associated with OMCs is similar to the Reynolds scale separation discussed in Lecture I. An atmospheric quantity ϕ (wind components, temperature, water vapor) is separated into a large scale component $\overline{\phi}$ (e.g. explicitly resolved by a GCM), a mesoscale component ϕ' and a turbulent component ϕ'',

so that

$$\phi = \overline{\phi} + \phi' + \phi'' \tag{10}$$

One difficulty which immediately arises is in the scale separation. If L_s is the typical length scale for the surface heterogeneity (e.g. the width of the dry and wet patches), it has been shown that, for background winds of less than 10 m/s, OMCs develop for L_s in the range of 10 to a few hundred km (Yan and Anthes 1988, Zeng and Pielke 1995). Therefore, at the large scale end, the scale of the circulations becomes comparable to the resolution of three dimensional climate models, and in fact to the scale of synoptic processes. The assumption of scale separation is thus somewhat weak. On the other hand, relatively high model resolution, of the order of 10 km is needed to realistically simulate the structure of OMCs, so that a scale of typically a few tens of km could be taken as typical of the mesoscale component in Eq. (10).

The vertical flux of ϕ, F_ϕ is thus given by

$$F_\phi = w\phi = \overline{w}\overline{\phi} + \overline{w}\phi' + \overline{w}\phi'' + w'\overline{\phi} + w'\phi' + w'\phi'' + w''\overline{\phi} + w''\phi' + w''\phi'' \tag{11}$$

where the vertical velocity w has been also separated according to Eq. (10). When averaging over the large scale (or resolvable GCM scale) terms 3, 6, 7, and 8 disappear based on the definition of turbulent component (see Lecture I) which applies in our case to both the large scale and mesoscale circulations. The further assumption that OMCs are not explicitly resolved by GCMs leads to neglection of the terms 2, 4 and 7, so that we are left with

$$F_\phi = \overline{w}\overline{\phi} + w'\phi' + w''\phi'' \tag{12}$$

The first term in Eq. (12) is the vertical flux associated with large (resolvable) scale motions, the second is associated with OMCs and the third is due to turbulent motions. The problem is thus to quantify and possibly parameterize the second term in Eq. (12).

The following results are taken from the recent work of Seth and Giorgi (1995), who performed a 30-day simulation of OMCs with the three dimensional mesoscale model of Giorgi et al. (1993a,b). The fields necessary to drive the model were taken from ECMWF analyses of observations over the central-eastern U.S. for June 1990. Two experiments were performed, a control run in which the whole domain was covered by wet forest and a perturbed run in which a strip of dry grass of 200 km width extending in the north-south direction was surrounded by wet forested areas. The mesoscale fluxes and circulations were calculated as the difference between the perturbed vs control runs.

Figures 3.6a-c,show east-west cross-sections of the difference between perturbed and control run for u component of the wind, temperature and humidity at 3 pm of day 11 of the simulation, when strong OMCs were simulated by the model. The zonal wind component shows the formation of two sea-breeze-like circulations at each edge of the

dry strip, counterclockwise at the eastern edge and clockwise at the western edge, with ascending motion over the dry grass strip and descending motion over the wet areas. These circulations are in response to the low level heating over the dry grass (see Fig. 3.6b). Note that for moisture we find negative mesoscale moisture signal in the lower PBL regions over the low evaporating grass areas, with regions of positive mesoscale humidity signal aloft. This is caused by the ascending motions over grass which carry relatively moist low level air into the drier upper levels. Similarly, the ascending motions produce a negative temperature signal above the PBL over grass. This is due to the transport of lower potential temperature air into regions of higher potential temperature aloft (the mid-troposphere is on average statically stable).

A measure of the intensity of the OMCs is given by the circulation integral, C, along a closed path encompassing the OMC, i.e.

$$C = \oint V - dl \tag{13}$$

which for the model translates into

$$C = \int_{z_1}^{z_2} [w(x_2, z) - w(x_1, z)]dz + \int_{x_1}^{x_2} [u(x, z_2) - u(x, z_1)]dx \tag{14}$$

where x_1, x_2, z_1, z_2 are the corners of a square integral path. For the present calculations, z_1 and z_2 are chosen at about 300 m and about 2500 m, respectively, while x_1 and x_2 are chosen to encompass only the circulation at the eastern edge of the strip. Figure 3.7 shows the evolution of C (calculated after averaging the wind along the north-south direction) for the 30-day run. From this figure we see that a diurnal cycle for circulation is found nearly every day in response to day-time heating, and that on three days the circulation is close to 1×10^6 m^2/s, which is a typical intensity of a mid-latitude sea breeze. On these days, conditions are particularly favorable for OMC formation, with low background wind and high insolation (i.e. low cloud amounts). Strong background winds tends to destroy the OMCs and the presence of cloudiness decreases the surface heating and thus the main mechanism which maintains the OMCs.

Figure 3.8 shows the (inner) domain-average profiles of mesoscale and turbulent vertical fluxes (positive upward) of momentum, heat and moisture at 3 p.m. averaged for the 30 day simulation. The turbulent fluxes are derived from the diffusive PBL scheme used in the model. It is found that while the mesoscale momentum and, especially, heat fluxes for the present experiment are smaller than the turbulent fluxes, the mesoscale moisture fluxes are similar in magnitude, but different in vertical structure compared to the turbulent fluxes. On day 11 of the simulation, when the OMC has maximum intensity, the mesoscale fluxes had a more pronounced effect than for the 30-day average.

Thus, confirming earlier results with more idealized model configurations, the study of Seth and Giorgi (1995) indicated that, also in realistic atmospheric conditions, surface-forced OMCs can significantly affect the vertical fluxes of at least moisture and momentum. We don't have time here to discuss the effects on precipitation, but early studies by Yan and Anthes (1988) and also the experiments of Seth and Giorgi (1995) showed that under suitable conditions (convectively unstable profiles), precipitation can be triggered at the breeze upwelling front.

The questions remain of the climatological significance of OMCs and the possible parameterization of their effects within large scale GCMs. A framework for parameterizing OMCs effects has been proposed by Zeng and Pielke (1995) and Lynn (1994) using similarity theory. This consists of identifying a set of basic quantities which determine OMC formation and development, grouping them into non-dimensional parameters and then seeking empirical relationships between these parameters based on series of model simulations. For example, Zeng and Pielke (1995) identify five dimensionless paramers: the dimesionless height (ζ), the aspect ratio between the PBL height and L_s (ℓ), the Richardson number (Ri_B), the ratio of eddy turnover time over advection time (λ_1) and the ratio of kinetic energy of the large scale flow over the horizontal pressure gradient which results from differential heating (λ_2). These parameters are then combined to describe the vertical structure of the mesoscale momentum, heat and water vapor. The parameterized dimensionless total mesoscale fluxes (F_m) proposed by Zeng and Pielke (1995) have the form

$$\frac{F_m - f(\zeta)}{f(\zeta)} = [a_1 + a_2 p_1 + a_3 p_1^2 + a_4 p_2 + a_5 p_2^2 + a_6 p_3 + a_7 p_3^2] + [b_1 + b_2 p_1 + b_3 p_1^2 + b_4 p_2 + b_5 p_2^2 + b_6 p_3 + b_7 p_3^2]\zeta \quad (15)$$

where

$$f(\zeta) = e_1 + e_2\zeta + e_3\zeta^2 + e_4\zeta^3 \quad (16)$$

and $p_i (i = 1, 2, 3)$ represent three combinations of the five basic dimensionless parameters, which are different for mesoscale sensible heat, moisture and momentum fluxes. The values of the coefficients a_i, b_i, e_i in Eqs. (15) and (16) and the parameters p_i are found through empirical fits to results from a set of model simulations in which different geometries of dry and wet land are used (strips or alternating bands of width L_s).

The similarity approach to mesoscale flux parameterizion is in some way justified by the study of Zeng and Pielke (1994) who found in 2D model simulations that for background winds of less than 10 m/s, L_s greater than 10 km and summer conditions, OMC formation and characteristics showed a good level of predictability and little sensitivity to small initial perturbations. However, both in the study of Zeng and Pielke (1995) and Lynn (1994) idealized surface geometries and atmospheric forcings were used, e.g. regular patches, constant wetness factors, homogeneous winds and simple vertical atmospheric temperature

and moisture profiles. Therefore, although the non dimensional expressions found in these studies indicate the existence of basic relationships between OMC, surface forcings and atmospheric conditions, they are likely not applicable to the real atmosphere, when much more complex atmospheric conditions and patterns of surface forcings are present. A much more extended number of realistic simulations such as those os Seth and Giorgi (1995) is needed to develop parameterizations of OMC effects.

A few comments are finally useful on the observational evidence of the existence of OMCs generated by vegetation discontinuities. Observations of such circulations are still scanty and not adequate for an assessment of their climatological importance. However, some field experiments have provided interesting indications. For example, the HAPEX-MOBILHI experiment in south-western France (Andre et al. 1986, 1988; Mascart et al. 1991, Bougeault et al. 1991) showed evidence of the existence of OMCs between a forest and agricultural areas. Segal et al. (1989) observed a significant difference in turbulent activity, air temperature and water vapor in the lowe boundary layer between irrigated areas nd surrounding dry land. More recently, Mahrt et al. (1994) observed a cool moist inland breeze which flowed outward from the center of an irrigated area during the California Ozone Deposition Experiment. This evidence is still inconclusive, however it should be kept in mind that OMCs of different origin, such as sea and lake breezes, and slope and urban island circulations are well known to occur with regularity and to significantly affect climate regionally (e.g. Atkinson 1981, Giorgi and Mearns 1991). Therefore, even if the global impact of OMCs is not large, their effect can be significant on the regional scale and may thus need to be accounted for in climate simulations applied to regional studies.

3.5. Summary considerations

The modeling activities described in this section clearly indicate that surface heterogeneities have significant effects, both direct and indirect, on the surface water and energy budgets and on the exchanges of momentum, energy and water vapor between land and atmosphere. Many attempts at understanding, quantifying and including these effects in ESEMs are currently under way. However, these attempts are undermined by the lack of adequate observational data, a feature quite common in the study of surface processes. The description of surface heterogeneity effects in climate models and the assessment of their climatic significance is an area of research which is still in it's beginning stages and, as human activities keep modifying the characteristics of the surface on wide ranges of spatial scales, it will likely remain of much interest in the next years within the global change debate.

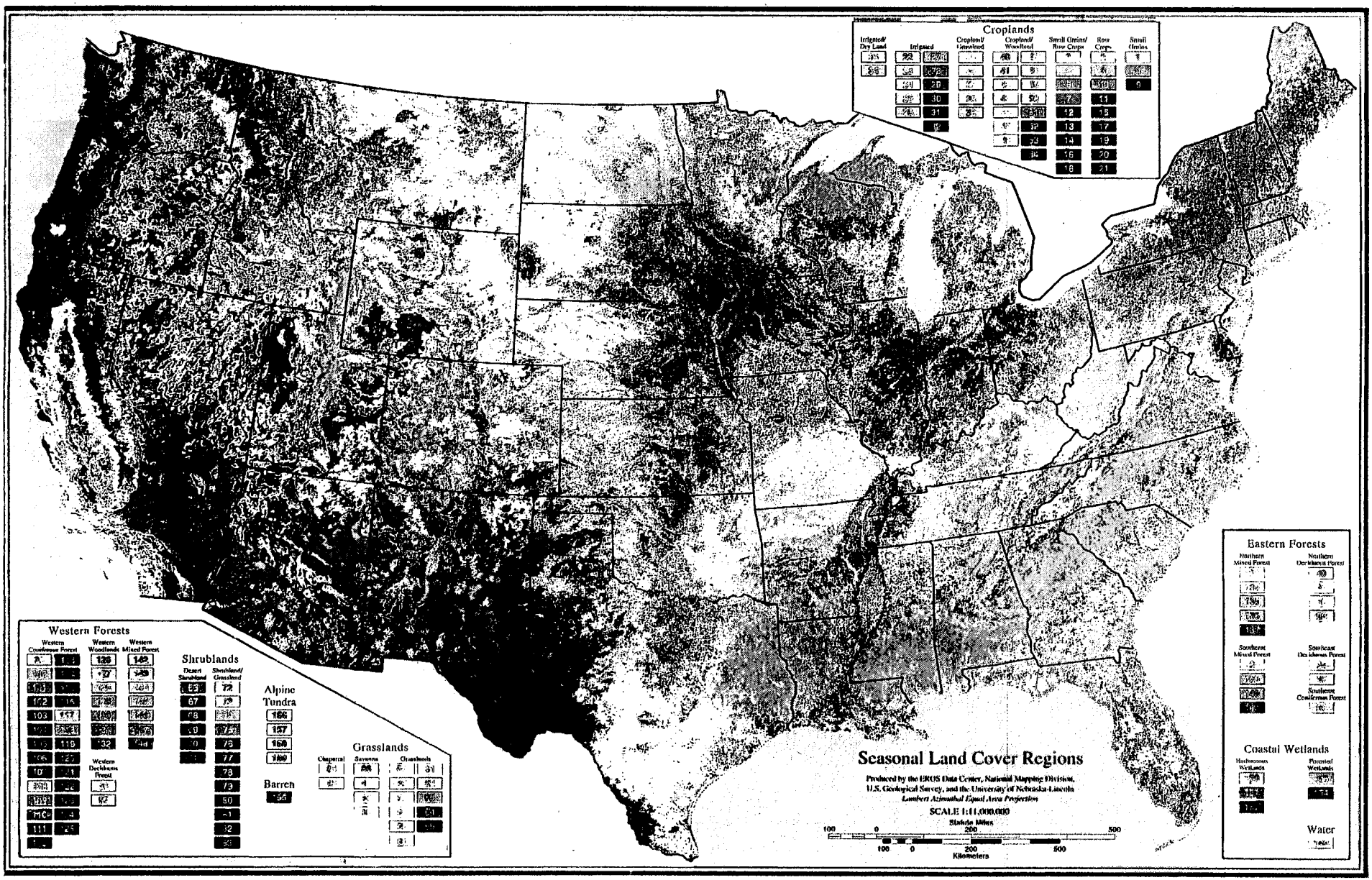

Fig. 3.1 Land surface type over the continental U.S.

300 Km

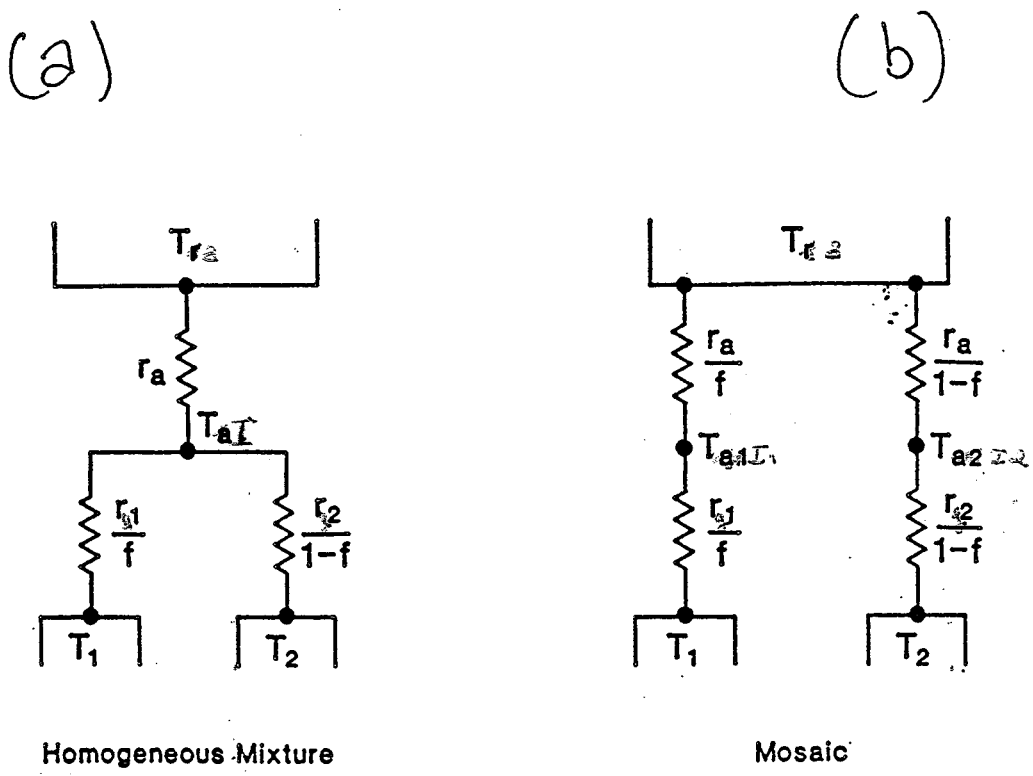

Figure 3.2 Resistence networks for idealized "mixture" (a) and mosaic (b) modeling approaches

$$\overline{F}_T = \frac{T_s - T_a}{r_a} = \sum_i \frac{f^i}{r_s^i} \left(T_s^i - T_1\right)$$

$$\overline{F}_T = \sum \frac{f^i}{r_a^i + r_s^i} \left(T_s^i - T_a\right)$$

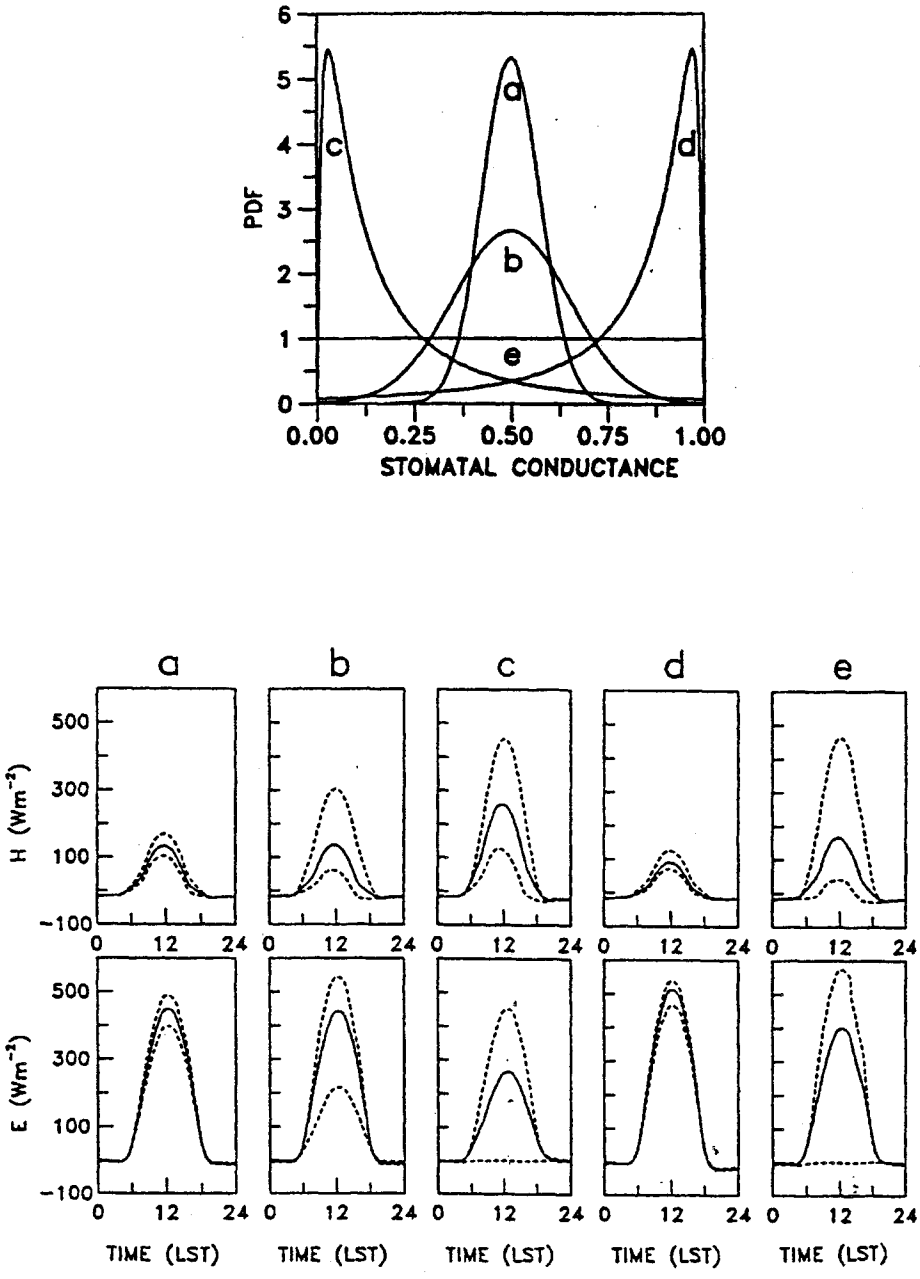

3.3

Figure 5 The impact of five different PDFs of stomatal conductance on the diurnal variation of surface sensible heat flux H and latent heat flux E. Solid lines represent grid global values and dashed lines indicate maximum and minimum values obtained in the grid element. The 5 PDFs are given in the top panel. (From Avissar 1992).

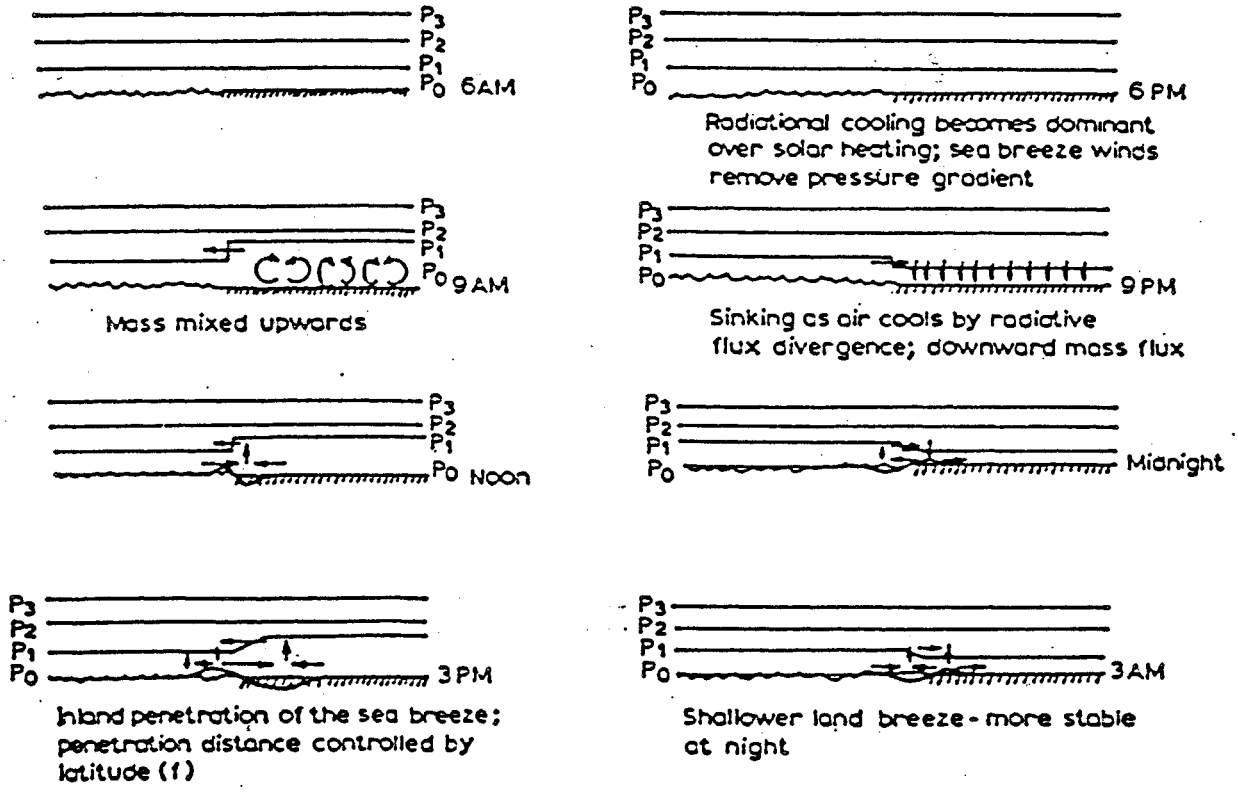

Figure 3.4 A schematic representation of the diurnal evolution of a land-sea-breeze.

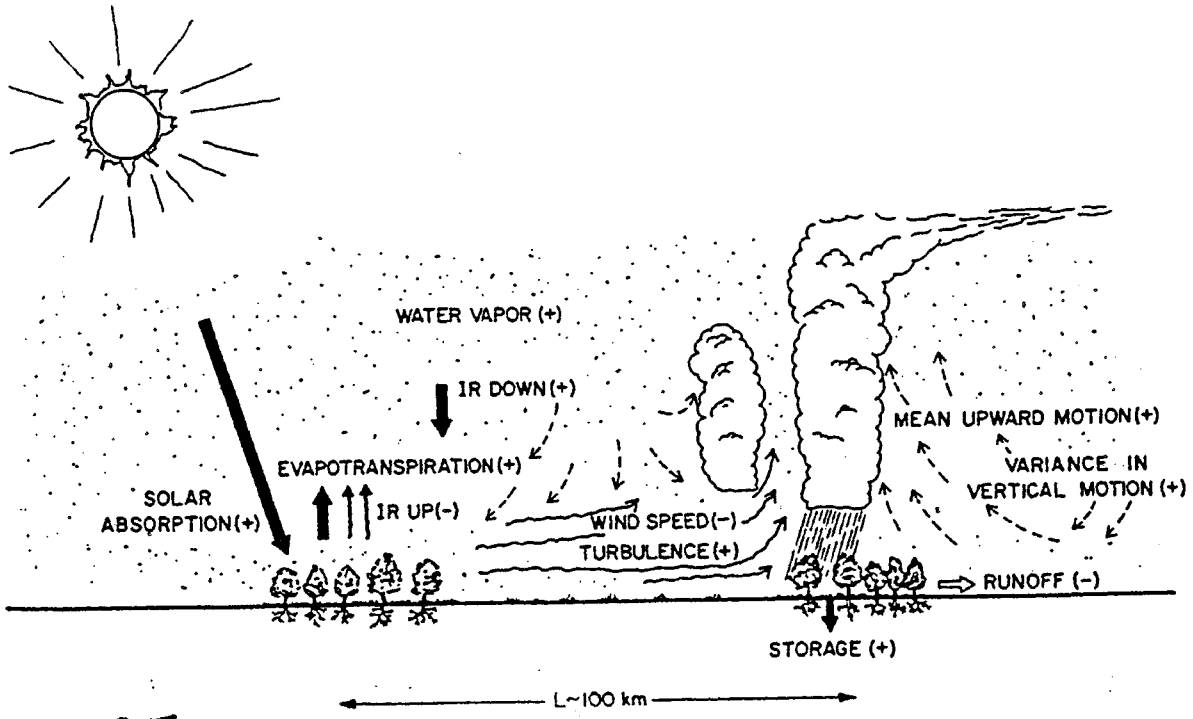

3.5

Figure 8. Hypothesized effect of establishing bands of vegetation in a semi-arid region of previously bare soil. Increases or decreases of an effect or process following the introduction of vegetation are indicated by pluses or minuses, respectively. (From Anthes 1984).

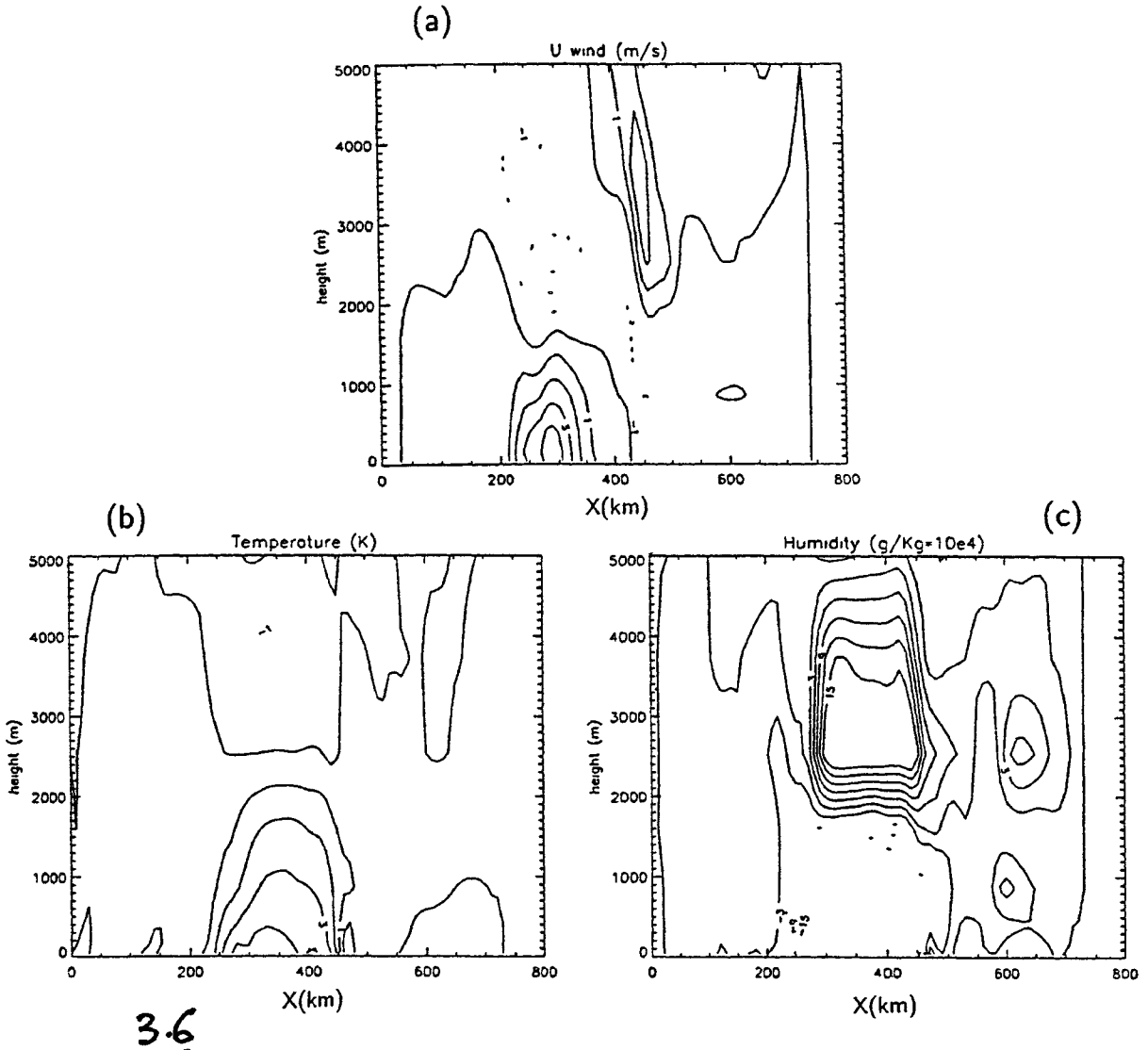

3.6

Figure 11 Two-dimensional west-east cross section, averaged in the north-south direction, of (a) horizontal u wind, (b) air temperature and (c) humidity differences between the control and perturbed experiments of Seth and Giorgi (1996) at 3 p m of day 11 of simulation

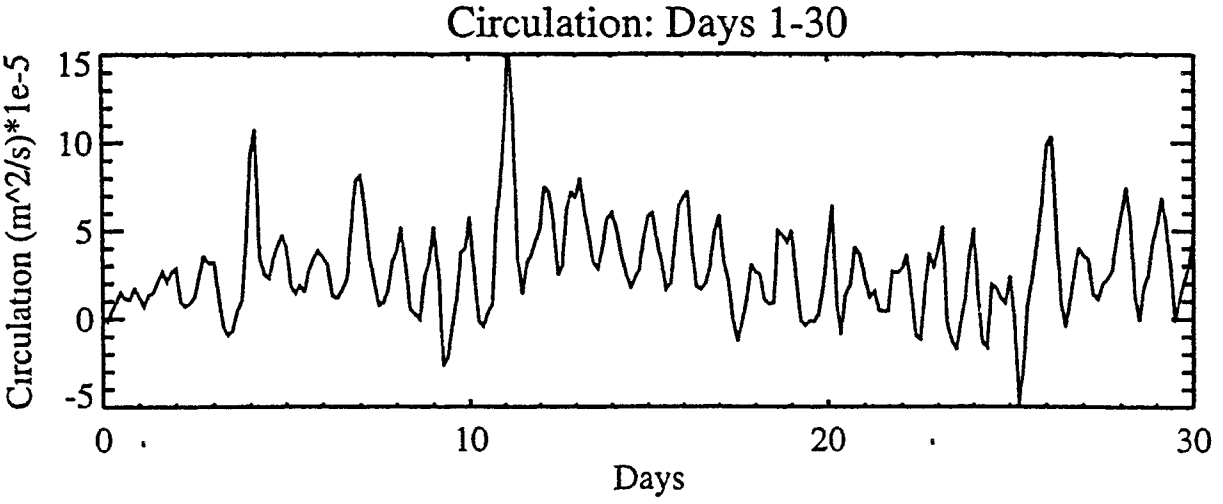

3.7

Figure 11 Time series of circulation computed from perturbed minus control run differences in horizontal u wind at the eastern edge of the dry strip of Fig 9 in the experiments of Seth and Giorgi (1996)

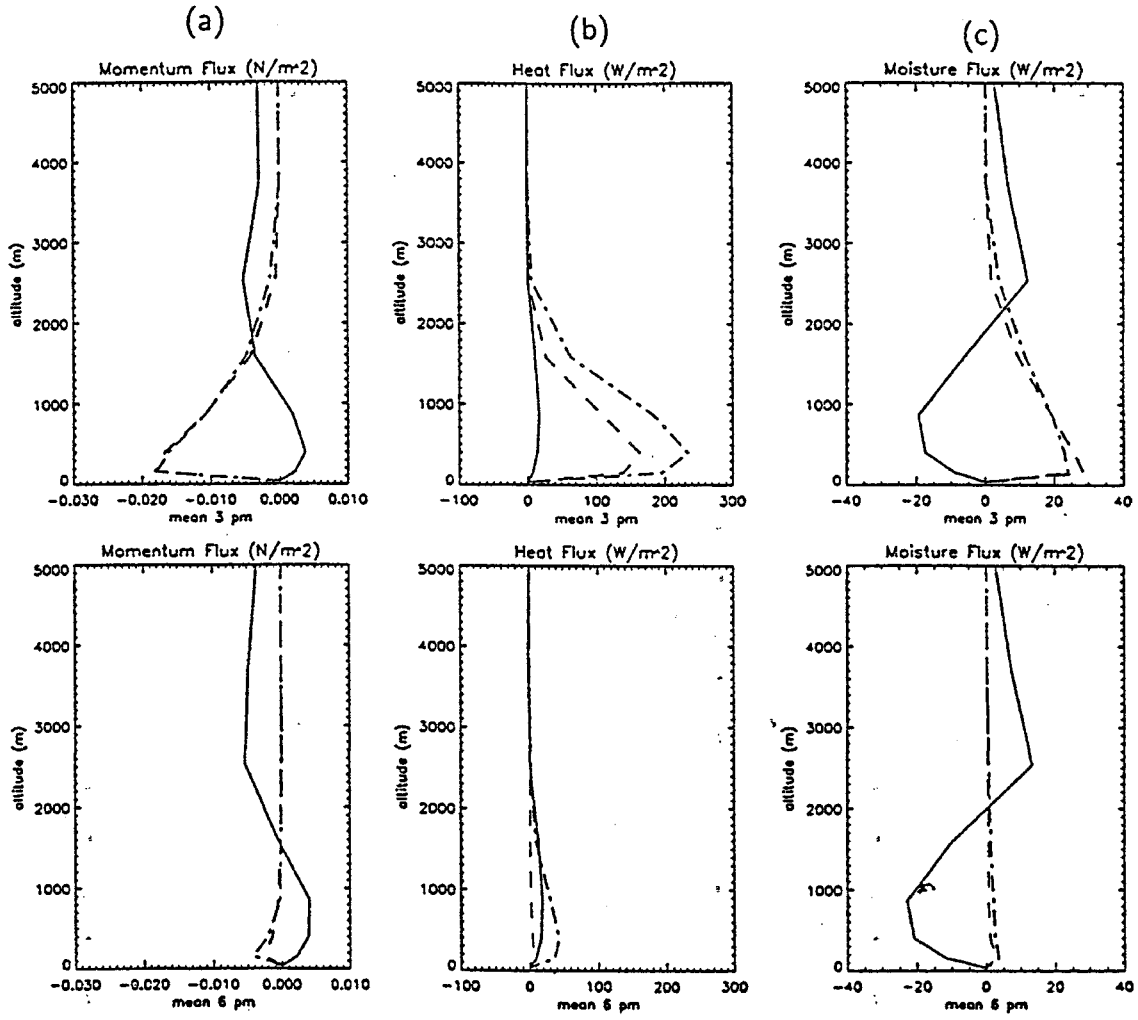

Figure 3.8 vertical profiles of mesoscale (solid) vs. turbulent fluxes (dash-dot), (a) momentum, (b) heat, (c) moisture, time means at 3 and 6 pm over 30 days.